



# Data modeling and assimilation studies with the MU radar

Shun-Rong Zhang<sup>a, b, \*</sup>, Shoichiro Fukao<sup>a</sup>, William L. Oliver<sup>c</sup>

<sup>a</sup>Radio Atmospheric Sciences Center, Kyoto University, Uji, Kyoto, 611-0011, Japan

<sup>b</sup>Wuhan Institute of Physics and Mathematics, CAS, P. O. Box 71010, Wuhan, 430071, Peoples Republic of China

<sup>c</sup>Department of Electrical and Computer Engineering and Center for Space Physics, Boston University, Boston, MA 02215, USA

Received 15 October 1998; received in revised form 1 April 1999; accepted 16 April 1999

## Abstract

We report initial results of data modeling and assimilation studies for several MU radar experiments. Various inputs to a one-dimensional ionospheric model are adjusted to provide agreement with observation and also to learn the sensitivity of the model to their variations. Certain observations are also used directly in the model to anchor or constrain its behavior. In particular, studies of the electron density from 100 to 500 km altitude in the ionosphere are carried out with the help of a theoretical model of  $O^+$ ,  $NO^+$ ,  $O_2^+$  and  $N_2^+$  densities and MU radar observations of the power, ion-drift and plasma-temperature profiles. Four typical cases are selected to study quantitatively the effects of the (A) perpendicular-north component of the plasma drift (15 December 1986), (B) atmospheric composition (7 October 1986), (C) solar EUV flux (2 August 1989) and (D) upper-boundary  $O^+$  density (5 October 1989) on the model  $N_mF2$ ,  $h_mF2$  and  $N_e$  profile, as well as on the neutral wind calculation from  $h_mF2$  and drift data. It is found that the measured vertical ion drift explains quantitatively well the measured  $h_mF2$  (particularly at low solar activity) while the model gives a better match with the measured  $N_e$  when it uses the  $h_mF2$ -based wind rather than the measured plasma drift. Different model values of the atmospheric  $O/N_2$  ratio and EUV flux and different values of the upper-bound  $O^+$  density may modify not only  $N_mF2$  markedly but also  $h_mF2$ : a lower  $O/N_2$  ratio results in higher  $h_mF2$ ; the EUVAC model gives higher  $h_mF2$  at high solar activity than does the EUV91 model; with a smaller upper-bound  $O^+$  density,  $h_mF2$  is lower by day but little changed by night. We specifically note that the meridional wind needed by the model to reproduce the observed  $h_mF2$  differed according to how well the model reproduced the observed  $N_mF2$ . The uncertainties in the MSIS86 and EUV model predictions are also discussed. It is found that if the MSIS and EUV91 models are used together, the model gives an  $N_mF2$  higher than that measured at high solar activity. Thus the  $O/N_2$  ratio needs to be reduced from the MSIS value if EUV91 is used. If EUVAC is used, no large modification is required. At equinox for low solar activity, modeling with either EUV model produces  $N_mF2$  values lower than those measured, and so the true  $O/N_2$  ratio may be higher than that given by MSIS model. © 1999 Elsevier Science Ltd. All rights reserved.

## 1. Introduction

A number of sophisticated theoretical (or first-principle) models have been proposed to develop our

understanding of the physical and chemical processes taking place in the upper atmosphere, and many observed ionospheric features have been explained qualitatively through their use. In contrast, small but physically detailed models, such as one-dimensional, non-self-consistent, and non-coupled models, sometimes exhibit advantages in modeling the ionosphere at a specific location under a specific set of solar-geophysical conditions. These latter models, however, often

\* Corresponding author. Tel.: +81-774-38-3845; fax: +81-774-31-8463.

E-mail address: shunrong@kurasc.kyoto-u.ac.jp (S.-R. Zhang)

depend on external empirical inputs of great uncertainty which may contribute greatly to departures between model and observation.

The solar extreme ultraviolet (EUV) radiation, which is highly variable in intensity during the solar cycle, provides the primary production for the ionospheric E and F layers (Hedin, 1988). The EUV91 model (Tobiska, 1991), the EUVAC model (Richards et al., 1994a) and the modified Hinteregger model (Richards and Torr, 1988) have recently been used widely in aeronomic calculations. Most theoretical ionospheric models that do not include a self-consistent atmosphere adopt an empirical atmospheric model, such as the Mass-Spectrometer Incoherent-Scatter (MSIS) model, which has been developed since the 1970 s. The MSIS86 model (Hedin et al., 1991) is believed to give a good representation of the atmospheric composition and temperature in an average sense. However, it was found that although MSIS predicts oxygen density in agreement with long-term observations of incoherent scatter (IS) radars, the radar records at Millstone Hill have shown the oxygen density to have episodic departures from the MSIS values reaching amplitudes of up to 50% and lasting for periods of several months (Oliver and Glotfelty, 1996). Buonsanto et al. (1992) also introduced modifications to MSIS composition to gain reasonable electron density in the E layer. The best available empirical horizontal wind model HWM has been created by Hedin et al. (1991). There are a number of comparisons of model winds with directly observed winds as well as with those derived from the ionospheric F2 peak height  $h_mF2$  (e.g. Titheridge, 1993; Igi et al., 1996). In general, the results suggest the necessity of further improvements for the model. The uncertainty in the wind specification for modeling has been greatly reduced since methods of deriving equivalent winds from  $h_mF2$  were developed by Miller et al. (1986), Buonsanto et al. (1989), and Richards (1991). Comparisons of these methods are discussed by Buonsanto et al. (1997).

Modeling efforts are advancing to the stage of not only qualitative but also quantitative agreement. Richards et al. (1994b) made comparisons of theory and measurement for the F2 peak electron density at Millstone Hill and Hobart. They used EUVAC, MSIS, and  $h_mF2$ -based winds to perform realistic modeling with the FLIP model (Richards and Torr, 1988). Pavlov and Buonsanto (1997), Mikhailov and Foster (1997) and Richards and Wilkinson (1998) have developed approaches to determine the error in MSIS model predictions by comparing the results of theoretical models with electron densities measured by ionosonde and Millstone Hill IS experiments.

The MU radar, located at Shigaraki (34.85° N, 136.1° E), is a large atmospheric radar capable of

detecting the Incoherent Scatter (IS) from the free electrons in the ionosphere. Since its initial IS operation in December 1985, a lot of interesting information on ionospheric electron density ( $N_e$ ), neutral wind and electromagnetic drift, and electron and ion temperatures ( $T_e$  and  $T_i$ ) has been published. Rishbeth and Fukao (1995) gave a review of these thermospheric and ionospheric results. Fukao et al. (1996) reviewed the ionosphere-thermosphere coupling as elucidated by the MU radar IS observations. More recently, Su et al. (1997) modeled the ionospheric electron density and temperatures over the radar using the Sheffield University Plasmasphere-Ionosphere Model (SUPIM). Balan et al. (1997) investigated the annual variation of the electron density. In general, such modeling work for the Asian Sector, and the consequent validation of atmospheric models for this sector, has been very limited.

This paper carries out a somewhat realistic modeling study of ionospheric electron density by using the MU radar IS observations of the power, ion-drift and temperature profiles. The main purpose of the study is to determine quantitatively the sensitivity of the model to various physical processes, singly and jointly: the sensitivity to different drift components, the sensitivity to changes in atmospheric composition, the sensitivity to changes in solar EUV flux, the sensitivity to changes in the model upper boundary condition, etc. How these processes affect the electron density ( $N_mF2$ ,  $h_mF2$  and the  $N_e$  profile) and the deduction of the neutral wind from data are discussed. Also discussed are the adequacies of the empirical MSIS86 and EUV flux models for representing conditions above the MU radar. This study represents our initial step in the study of data assimilation into our model. This initial step addresses model sensitivity to various inputs; it does not yet address the uniqueness with which these contributions may be determined. It explores the extraction of the physics from the data but does not yet attempt forecasting from these deductions. Four typical cases are studied. We first give a brief description of how the data used here were obtained with the MU radar, then we describe a midlatitude ionospheric model and discuss the relevant aspects of that model construction. In the later two sections of this paper we present and discuss model results for the four individual cases. The last section gives a summary of our investigation.

## 2. MU radar data

A detailed description of MU radar IS measurements has been given by Sato et al. (1989), who describe the radar capabilities and compare these with the capabilities of other IS radars, and by Fukao et al. (1990), who report later improvements for ionospheric

temperature and drift-velocity measurements. Here we describe only how those measurements relevant to this study are obtained.

F-layer measurements are made with a 1-h cycle. In the first 15 min the radar measures power profiles with 9.6-km range resolution, and in the remaining 45 min it measures either drift-velocity profiles with 38.4-km range resolution or temperature profiles with 14.4-km range resolution. The 15-min power data are usually integrated to obtain a single profile, and so are the 45-min velocity/temperature data. The radar beam is switched sequentially each interpulse period between geomagnetic north, east, south and west at 20° zenith angle. The vector drift velocity (components parallel and perpendicular to the geomagnetic field) is then determined from the combination of the four line-of-sight Doppler velocities. The four power and temperature profiles are averaged to yield a single vertical profile for each of these physical parameters.

For temperature experiments the lowest measurable altitude is 186.3 km. These data are usually integrated to 45-km height resolution, for which the expected error is about 5–20% for 1-h time integration. For velocity experiments the lowest measurable altitude is 117.8 km. These data are usually integrated to 38.4-km height resolution, for which the expected error is 5–10 m/s for average daytime electron densities and 1-h integration. To improve statistical accuracy, we have averaged the drifts over the altitude range 220–350 km for cases of low solar activity or 220–450 km for cases of high solar activity to give a ‘layer velocity.’ This is a crude attempt to keep the range of averaging somewhat centered on the layer peak, in consideration that  $h_mF2$  increases as solar activity increases.

In order to determine the electron density  $N_e$  from each 15-min power profile, the neighboring 45-min temperature ratio  $T_r = T_e/T_i$  profile can be used in principle. However, the 1-h observing cycle measures either temperature or velocity, never both, so the temperature information is not always available. In this study we use average  $T_r$  profiles, obtained from a data base of experiments, to derive  $N_e$ . Fortunately, this rarely leads to serious errors, for even were the temperature correction not made at all, an error of about 10% is all that is expected in most cases. The ionosonde maximum electron density  $N_mF2$  is used to calibrate the electron-density profile.

### 3. Model

#### 3.1. Model construction

Our present midlatitude ionospheric model is based upon previous work of Zhang et al. (1993, 1996) and Zhang and Huang (1995). The model solves the

equations of mass continuity and motion for  $O^+$  that consider gravity, pressure gradients and ion drag. The electric field effect is generally ignored, but when we use the observed drifts or  $h_mF2$ -based wind, it becomes included in an equivalent drift, which is described below.  $H^+$  and thermal diffusion effects are neglected, and this might be justified within the 100–500 km height range on which we will focus in this paper. Molecular ion ( $NO^+$ ,  $O_2^+$  and  $N_2^+$ ) densities are determined from photochemical equilibrium assumptions.

We have not introduced the equation of energy; therefore we use empirical or experimental temperatures.  $T_e$  and  $T_i$  influence both plasma diffusion and chemical reaction rates in our model. Even when they are assumed to equal the MSIS neutral temperature  $T_n$ , the model calculations for  $N_mF2$  and the  $N_e$  profile often remain reasonable over the 100–500 km height range. The ionospheric temperatures may also be provided by the International Reference Ionosphere (IRI) (Bilitza, 1990). Since the MU radar measures the temperatures only above 186.3 km altitude, temperatures below this altitude are taken from the IRI and adjusted to match the observed temperature at 186.3 km. In short, the model is designed to accept either MSIS86 neutral temperature, IRI temperatures, or the observed temperatures as  $T_e$  and  $T_i$  inputs.

The ion chemistry of the model involves 21 reactions for  $O^+(^4S)$ ,  $NO^+$ ,  $O_2^+$ ,  $N_2^+$ ,  $O^+(^2D)$  and  $O^+(^2P)$ , of which 13 concern the meta-stable species  $O^+(^2D)$  and  $O^+(^2P)$ . Branching of the  $O^+(^2D) + N_2$  reaction to  $N_2^+$  and  $O^+(^4S)$  is thought to be important for the ionospheric F1 region, although the branching rate still seems poorly known. Here we take  $10^{-10} \text{ cm}^{-3} \text{ s}^{-1}$  to be the rate coefficient for this reaction (see Torr and Torr, 1982). Details for the chemical reaction scheme and rates can be found in Zhang and Huang (1995).

The ionization of a neutral particle by solar EUV irradiation produces a primary photoelectron that may retain sufficient energy to produce secondary ions. It was found that photoelectron impact ionization could increase the total production by 30% between 150 and 250 km (Torr and Torr, 1979) or even more (Lilensten et al., 1989). Due to the complexity of a full calculation many ionospheric models use simple mean models to allow for the impact effect. Richards and Torr (1988) gave formulae for the ratio of secondary production to photoionization. Titheridge (1996) developed an approach in which a secondary ionization factor is determined for each ion species in each solar wavelength band. We provide access to both photoelectron impact models. However, we find that the Richards and Torr (1988) formula generates good agreement between the model and observed  $N_e$  in the lower F2 region (as shown in the next section).

The photoionization production rates for  $O^+$ ,  $O_2^+$  and  $N_2^+$  as a function of height depend on solar radi-

ation flux, optical depth, photoionization cross section, ionization efficiency and concentrations of the neutral species O, O<sub>2</sub>, N<sub>2</sub>. The optical depth is obtained in this investigation by integrating numerically along the rays of sunlight, instead of by using the Chapman function. The 37 wavelength bands and the photoionization and photoabsorption cross sections are taken from Torr and Torr (1982). Solar EUV fluxes are taken from either the EUV91 or EUVAC model. EUV91 specifies the solar EUV irradiance for wave-lengths of 1.8–10.5 nm based on rocket and satellite data compiled between 1977 and 1988, while EUVAC specifies the 5–57.5 nm wavelength fluxes based on the F74113 solar EUV reference spectrum and relative variations of the EUV flux as measured by the AE-E satellite.

Atmospheric temperature and composition are taken from the MSIS86 model. However, as an averaged model, it must depart from the real situation even at geomagnetic quiet condition. In order to reproduce the observed ionospheric density, it is necessary to make modifications to the O/N<sub>2</sub> ratio of MSIS. The NO density (not included in the MSIS model) is calculated from the O and O<sub>2</sub> densities (Mitra, 1968).

Vibrationally excited N<sub>2</sub> also affects N<sub>e</sub>, especially in summer at high solar activity. The rate coefficient  $k$  for the reaction of O<sup>+</sup> with N<sub>2</sub> depends on the numbers of molecules in the various vibrational states. As a crude approach to allowing for this effect, the present model adopts the expression of Buonsanto (1995),  $k = k_0(T_f - 1000)/250$  for  $T_f > 1250^\circ\text{K}$ , where  $k_0$  is the rate coefficient for non-excited N<sub>2</sub> and  $T_f$  is an effective temperature defined by  $T_f = (7 T_i + 4 T_n)/11$ . No modification is made for  $T_f \leq 1250^\circ\text{K}$ .

The O<sup>+</sup>-O collision cross section (collision frequency) is of great importance in ionospheric dynamics and energetics. Many recent studies have suggested corrections to the often-used value of Banks (1966). In this investigation we assume a cross section a factor of 1.2 times Banks' value. As a matter of fact, the uncertainties in the collision frequency are not so important when we use an equivalent wind derived from  $h_m\text{F2}$  (Richards, 1991) as long as we use the same value in determining wind from the data and in applying wind forcing in the model.

To solve the O<sup>+</sup> diffusion equation, we must set upper and lower boundary conditions. We assume photochemical equilibrium to apply at the lower boundary (100 km). The upper boundary (500 km) condition may be specified by one of the following options: (1) the experimental O<sup>+</sup> density ( $=N_e$ ), (2) the IRI O<sup>+</sup> density, (3) an adjusted O<sup>+</sup> density, (4) O<sup>+</sup> fluxes (experimental, empirical or theoretical). The third option uses an O<sup>+</sup> density chosen to force agreement between the modeled and observed  $N_m\text{F2}$ .

The model uses time and height intervals of 2 km and 15 min. To ensure that model densities are not

influenced by chosen initial conditions, the model is run for 24 h prior to the time of the experiment.

### 3.2. Neutral wind

We now discuss the thermospheric winds used by the model. HWM90 is used as our default option. When we have external information on  $h_m\text{F2}$ , we can derive an 'equivalent' wind, based on the theory of how the wind affects the height of the F layer. Values of  $h_m\text{F2}$  can be derived from ionograms or from radar measurements of the power profile. There are two approaches to deriving an equivalent wind (vertical drift) from  $h_m\text{F2}$ : the first uses the 'servo-model' of the F layer (Rishbeth et al., 1978) (e.g. Buonsanto et al., 1989); the second uses a theoretical model, e.g. the FLIP model, to specify the relationship between the meridional neutral wind  $U$  and  $h_m\text{F2}$  (Miller et al., 1986; Richards, 1991; Miller et al., 1997).

We use our model to derive an equivalent wind from  $h_m\text{F2}$ . In contrast with both the servo-model and the FLIP-model approaches, we do not assume that changes in  $U$  are linearly proportional to changes in  $h_m\text{F2}$ . Rather, the equivalent wind is obtained directly by matching  $h_m\text{F2}$  by the model.

The MU radar measures the ionospheric drift components both parallel and perpendicular to the direction of the magnetic field. The parallel component  $v_{\parallel}$  and the perpendicular-north component  $v_{\perp}^N$  both contribute to the vertical drift  $v_z$ . The behavior of  $v_{\perp}^N$  over the MU radar has been studied by Oliver et al. (1993), Fukao et al. (1996) and Su et al. (1997). The vertical component of the drift can be expressed as  $v_z = v_{\parallel} \sin I + v_{\perp}^N \cos I$ , where  $I$  is the magnetic dip angle, therefore the southward wind can be expressed as  $u_s = (v_z / \sin I - v_d \sin I) / \cos I$ , where  $v_d$  is the upward diffusion velocity. The equivalent southward wind  $u_s$  therefore contains a contribution from  $v_{\perp}^N$ . In practice, by assuming an initial wind profile given by HWM90, we calculate  $N_e$  and thereby  $v_d$  and finally  $v_z$ . The model  $v_z$  is averaged over 220–350 km or 220–450 km, corresponding to the range used for MU radar drift averaging, and then compared to the averaged observed vertical drift  $v_z$ . The difference of the two averaged drifts,  $\delta V_z$ , provides a correction term  $\delta V_z / (\cos I \sin I)$  to the initial wind. Further calculations on this basis result in further correction (Su et al., 1997). Such an iterative process is found to converge rapidly.

### 3.3. The additional ionization source or sink

We note that even though most important parameters, such as ion drifts/ $h_m\text{F2}$ /winds, ionospheric temperatures and upper boundary O<sup>+</sup> density, could be determined by the measurements, model calculations still may not reproduce the observed  $N_m\text{F2}$ .

Table 1  
Model features

EUV model	(1) EUV91 (2) EUVAC
Photoelectron impact	(1) Richards and Torr (1988) (2) Titheridge (1996)
$T_n$ and O, N <sub>2</sub> , O <sub>2</sub>	MSIS86
$T_i$ , $T_e$	(1) $T_i = T_e = T_n$ (MSIS) (2) IRI90 (3) observation
Vibrationally excited N <sub>2</sub>	Buonsanto (1995)
Wind	(1) HWM90 (2) observed equivalent parallel drifts (3) $h_m$ F2-based equivalent wind, calculated by this model directly (see text)
Upper boundary (500 km) O <sup>+</sup>	(1) IRI90 O <sup>+</sup> (2) observed $N_e$ (3) O <sup>+</sup> flux (4) adjusted O <sup>+</sup> (see text)
Lower boundary (100 km) O <sup>+</sup>	Photochemical equilibrium
Matching F2 peak	$h_m$ F2-based wind; MSIS86 modification and/or additional ion source or sink

Reasons include the improper specification of the EUV flux and neutral composition, especially the atom/molecule ratio. Adjustment of these inputs is then necessary. Moreover, when necessary (see discussions afterwards), we introduce an additional ionization source or sink (AISOS) to further account for model-data departures. In contrast to the practice of Richards et al. (1995), we assume a single equivalent ionization source or sink value for all heights (100–500 km) at each time step, depending on whether the model  $N_m$ F2, is lower or higher than the measured one. This value is equal to  $\beta_m \delta N_m$ F2, where  $\beta_m$  is the O<sup>+</sup> loss frequency at the F2 peak and  $\delta N_m$ F2 is the  $N_m$ F2 data-minus-model difference.

The main features of the model are summarized as in Table 1.

#### 4. Modeling results and discussions

Four cases, listed in Table 2, have been selected for modeling on the basis of the quality of the data and a diversity of solar activity and season. The measured electron density at 500 km is utilized to determine the top boundary condition in all cases.

##### 4.1. Case A: 15 December 1986 (day 86349) winter, low solar activity

In this case we emphasize the difference in model

results incurred when we use (a) the full vertical drift  $v_z$  and (b) only the vertical component of the parallel drift  $v_{\parallel}$  measured by the radar. The latter choice ignores the electric-field.

##### 4.1.1. $h_m$ F2

The measured  $h_m$ F2 variation (triangle-line curve) may be considered typical for the winter low solar activity condition since it is well consistent with the IRI  $h_m$ F2 (square-line curve), which comes from a large volume of observations and gives a good representation of the average condition. It is seen that both the parallel drift,  $v_{\parallel}$  and vertical drift  $v_z$  bring the model and experimental  $h_m$ F2 into general agreement except for several hours at night when the model values underestimate the data. By night, the  $h_m$ F2 calculated from the  $v_z$  data (dotted line) is closer to the measurements than that calculated from  $v_{\parallel}$  data (dashed line); the east-west electric field induces a 20–30 km difference in  $h_m$ F2. By day, the difference is not significant (Fig. 1(a)).

##### 4.1.2. Wind

Winds may be computed from both  $v_z$  and  $v_{\parallel}$  (dotted and dashed lines Fig. 1(b)). The former is an equivalent wind containing a contribution from the north-perpendicular electromagnetic drift. The vertical component of the north-perpendicular drift is upward from midnight till sunset and down-ward at other times. The equivalent wind is very close to the empiri-

Table 2  
Four cases studied in this paper

Cases	Case A	Case B	Case C	Case D
Date	15 December 1986, day 86349	7 October 1986, day 86280	2 August 1989, day 89214	5 October 1989, day 89278
F107/F107A	71/72	74/76	202/217	218/223
Ap	4	5	6	5
Drift	Averaged over 220–350 km	Averaged over 220–350 km	Averaged over 220–450 km	Averaged over 220–450 km for 2–4 October
$T_e$ and $T_i$	IRI	IRI	Measured on 3 August	Measured

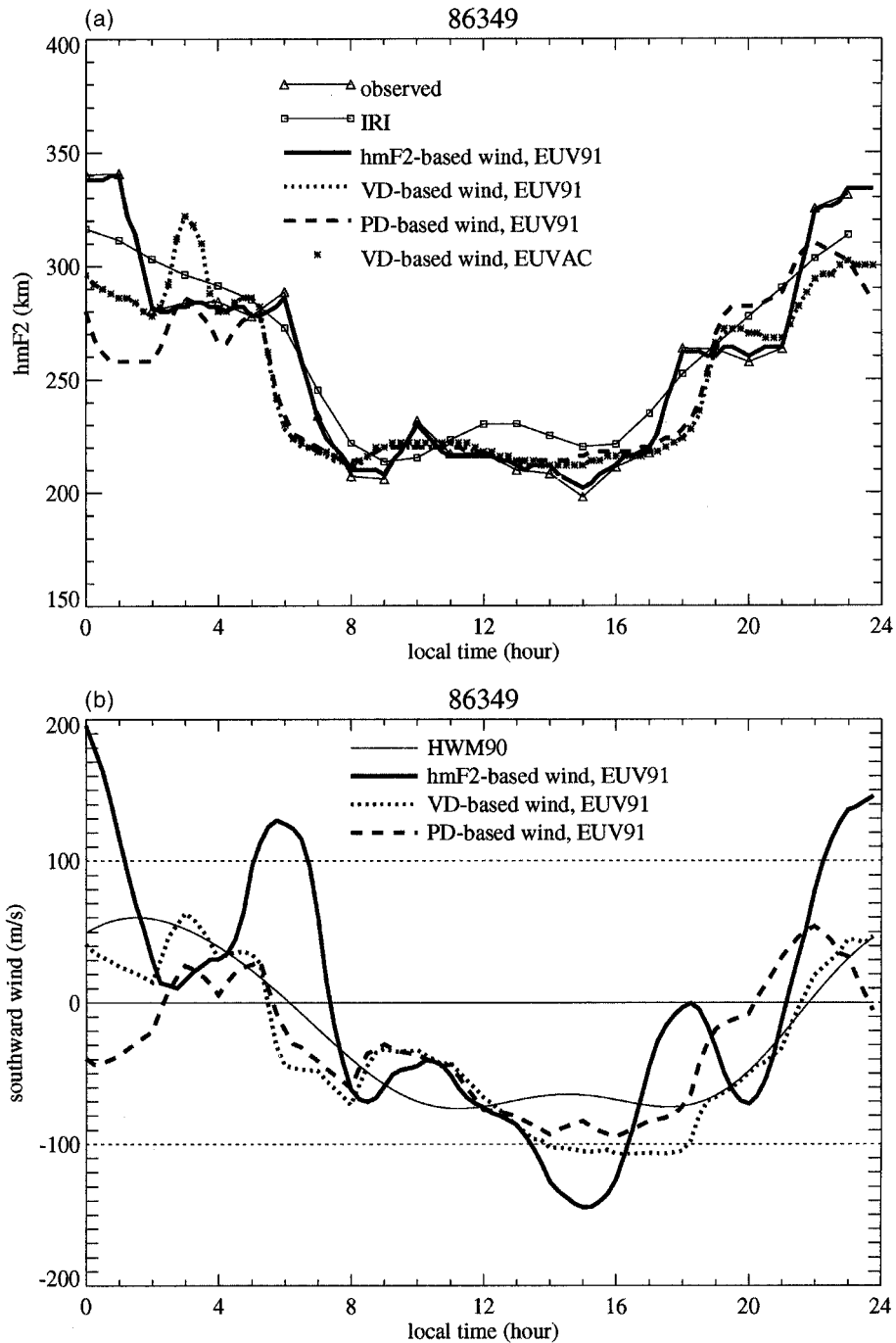


Fig. 1. Local time variations of (a)  $h_m F2$ , (b) the equivalent southward wind and (c)  $N_m F2$  for Case A (15 December 1986, day 86349). 'VD' stands for the measured vertical drift, and 'PD' stands for the vertical component of the measured parallel drift.

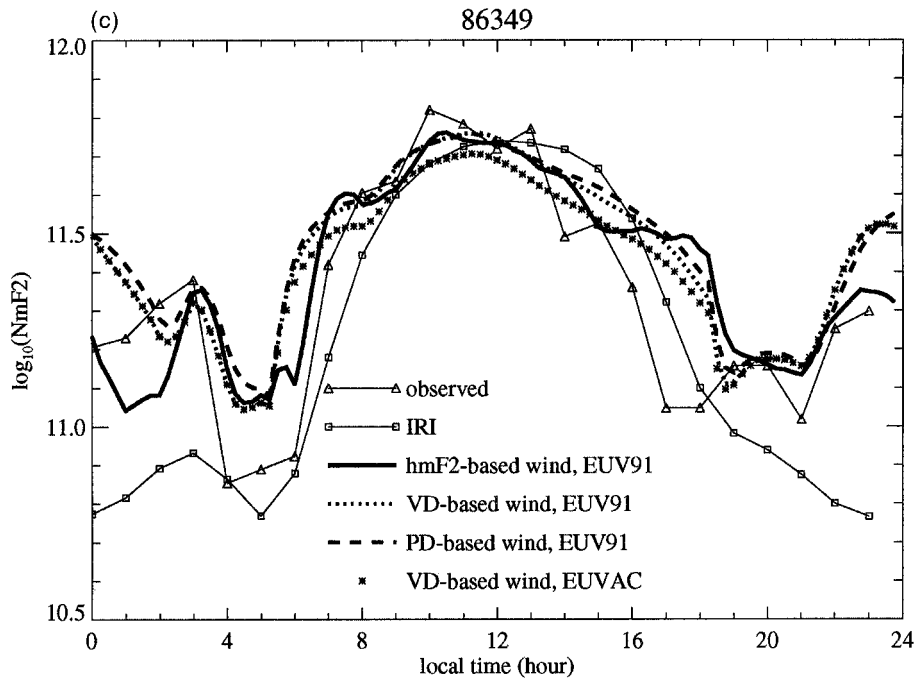


Fig. 1 (continued)

cal HWM90 wind. Also obtained is another type of equivalent wind (solid line) deduced directly from the observed  $h_mF2$ . Fig. 1(a) shows also how well the measured  $h_mF2$  is followed by the model  $h_mF2$  (solid line). (As a matter of fact, the observed  $h_mF2$  variations have been exactly rebuilt in all of our modeling cases by adjusting the equivalent wind; we will not show comparisons between these nearly identical  $h_mF2$  s hereafter.) The  $h_mF2$ -based equivalent wind and the  $v_z$ -based equivalent wind are similar at most times. The former exhibits large jumps around sunrise and sunset, meaning that the wind-induced drift is not effective in influencing  $h_mF2$  and that the wind derived from ionospheric height may not be reliable for those times. Additionally, the  $h_mF2$ -based wind becomes very large around midnight.

#### 4.1.3. $N_mF2$

The observed density and IRI density are very similar during daytime, but the IRI density is smaller at night. All wind options reproduce the observations well, with the  $h_mF2$ -based wind giving especially good agreement (Fig. 1(c)).

In Case A we have demonstrated the different model results obtained when we use  $v_z$ -based and  $v_{||}$ -based winds. In the following cases we will not discuss the  $v_{||}$ -based winds.

#### 4.2. Case B: 7 October 1986 (day 86280) equinox, low solar activity

##### 4.2.1. $h_mF2$ and $N_mF2$

The observed  $h_mF2$  is lower than the IRI  $h_mF2$  by 20–40 km except around 20:00 LT, and is characterized by peaks at around 03:00 LT and 20:00 LT (Fig. 2(a)). The model  $h_mF2$  resulting from use of  $v_z$ -based winds varies exactly as the observed  $h_mF2$  does, other than some constant offset, and the altitude peaks at 03:00 LT and 20:00 LT are correctly simulated. This model  $h_mF2$  is quantitatively closer to the IRI values than to the observed values except for the times of peaks. There are two possible reasons to explain why the model values are higher than the observed values: (1) the drift data have been averaged over 220–350 km to smooth out random errors; (2) plasma temperatures have been taken from IRI, thus if IRI predicts low electron temperature, the calculated  $h_mF2$  will be high. The  $h_mF2$ -based wind (Fig. 2(b)) is offset from the HWM wind by a large northward component.

The observed  $N_mF2$  shows a density depletion in the afternoon as compared to IRI predictions; from 05:00 LT until noon it is at the IRI density level. Modeling with the  $v_z$ -based wind gives an  $N_mF2$  smaller than the measured  $N_mF2$  before noon but larger after noon, while modeling with the  $h_mF2$ -based wind produces a

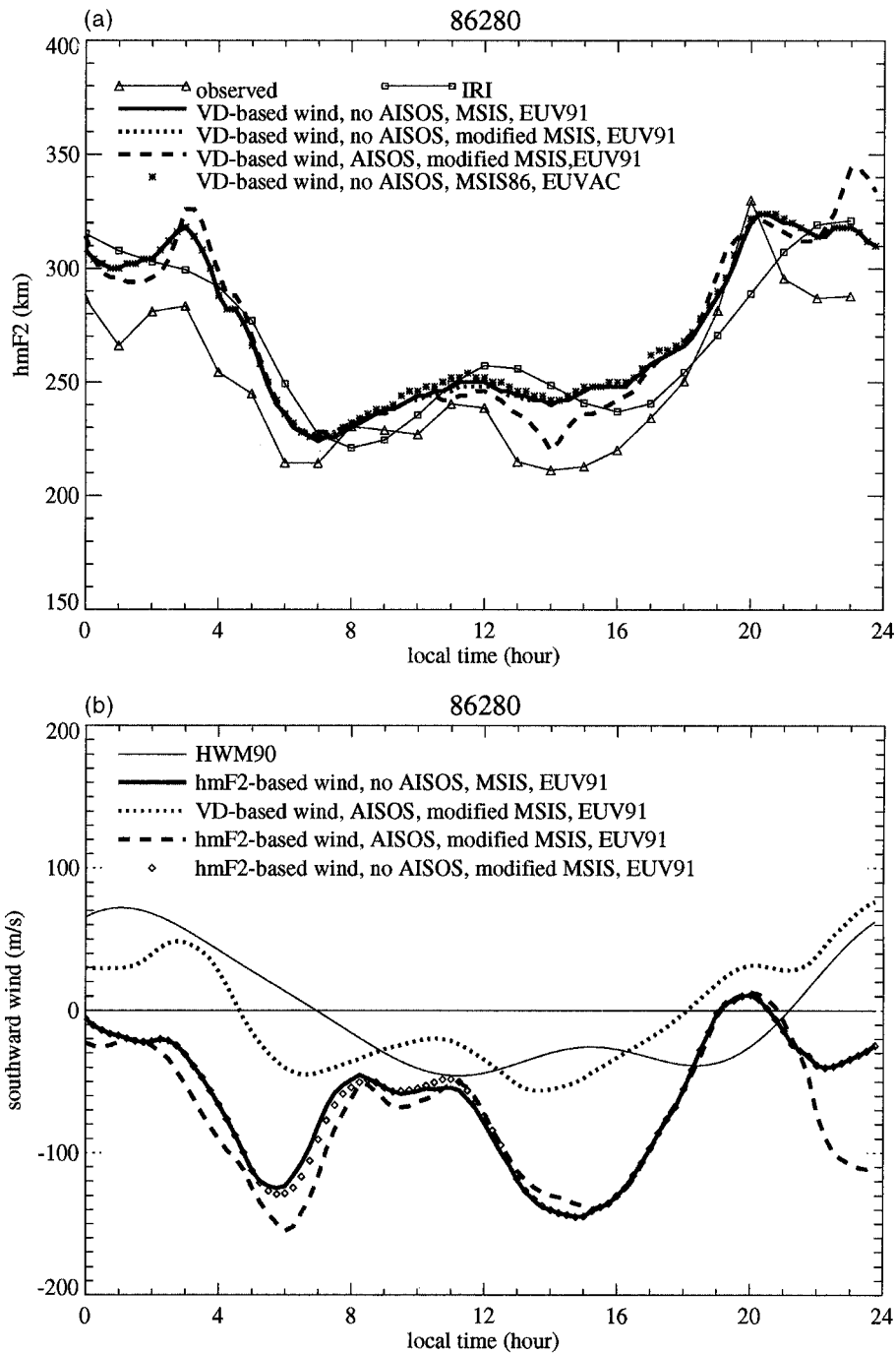


Fig. 2. Local time variations of (a)  $h_mF2$ , (b) the equivalent southward wind, (c)  $N_mF2$  and (d) the electron density profile for Case B (7 October 1986, day 86280). 'VD' stands for the measured vertical drift. 'AISOS' stands for additional ionization source or sink (see text). In (d), solid line: observation; dashed line: modeled with MSIS modification, AISOS,  $v_z$ -based wind; dotted line: the same as the dashed line except that the  $h_mF2$ -based wind is used.

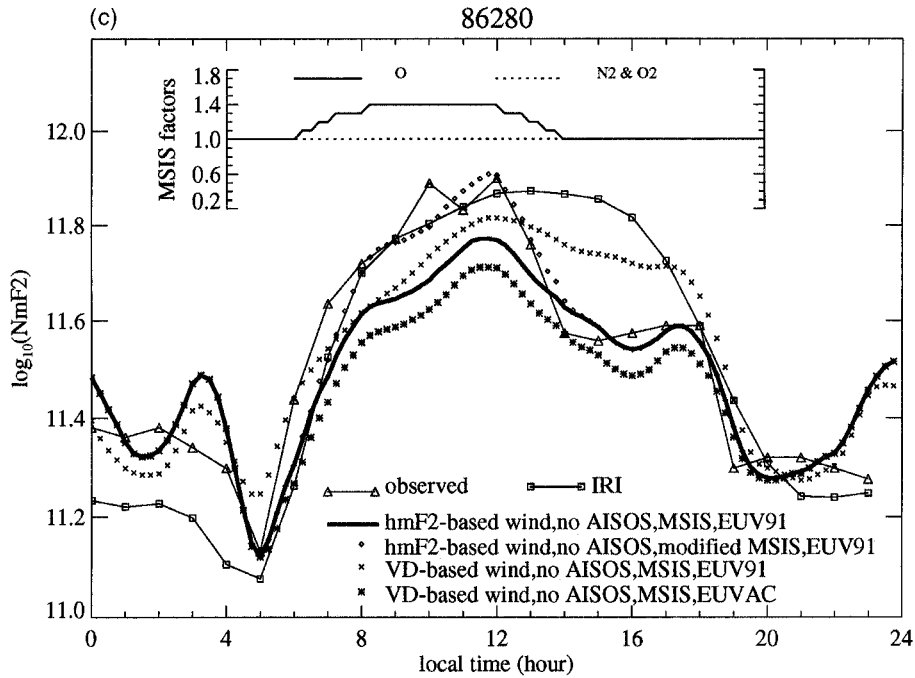


Fig. 2 (continued)

decreased  $N_mF2$  in the afternoon, in agreement with the observations. It can be expected that wind/drift dynamics plays a significant role in depleting the electron density in the afternoon.

#### 4.2.2. MSIS modification and the AISOS

However, for 05:00–13:00 LT the model gives a smaller electron concentration than the observation. This is true during the post-sunrise period, when composition is much more important than dynamics in determining density behavior (Rishbeth et al., 1995), suggesting that the MSIS model might have predicted a low O density. Now, suppose that the O concentration is increased by 40% over the MSIS level from 06:00–14:00 LT. As indicated in Fig. 2(c), the model  $N_mF2$  is significantly improved (diamond curve, using  $h_mF2$ -based winds). Meanwhile, the calculated wind (diamond curve, Fig. 2(b)) is not markedly affected.

To obtain better agreement in  $N_mF2$ , we introduce an additional ionization sink or source (AISOS), in addition to the MSIS modification. Model and data  $N_mF2$  can then be made to coincide (the corresponding model  $N_mF2$  is not shown in the plot as it would overlay the data). The AISOS production rate is shown in the next section.

The  $h_mF2$ -based wind, computed with the MSIS modification and AISOS, is stronger by 20–30  $m s^{-1}$  before 12:00 LT and 80  $m s^{-1}$  after 22:00 LT (dashed

line, Fig. 2(b)) than that obtained without the AISOS (diamond curve). The  $v_z$ -based wind, computed with the same MSIS modification and AISOS (dotted line), is closer to the HWM value but has a delay of 4 h in phase. The differences between the  $h_mF2$ -based and  $v_z$ -based winds are large and indicate complex control of  $h_mF2$  behavior.

Fig. 2(d) shows comparisons between the model  $N_e$  profile and the observed one (solid line) at each hour of the day. The model profiles are obtained for the  $v_z$ -based (dotted line) and  $h_mF2$ -based (dashed line) winds with the MSIS modifications and AISOS term applied. The observed profile is generally well reproduced by the model. The pre-noon enhancements below the F2 peak are not real but result from meteor-echo contamination in the experiment.

#### 4.3. Case C: 2 August 1989 (day 89214) summer, high solar activity

##### 4.3.1. $h_mF2$ and $N_mF2$

The observed  $h_mF2$  variation follows the IRI one in both phase and magnitude (Fig. 3(a)). The  $h_mF2$  measurements are reasonably reproduced by the model using the  $v_z$ -based winds (solid line), while the further inclusion of modifications of the O and  $N_2$  concentrations (Fig. 3(c)) and an AISOS gives better agreement with the data (dashed line). Especially by night

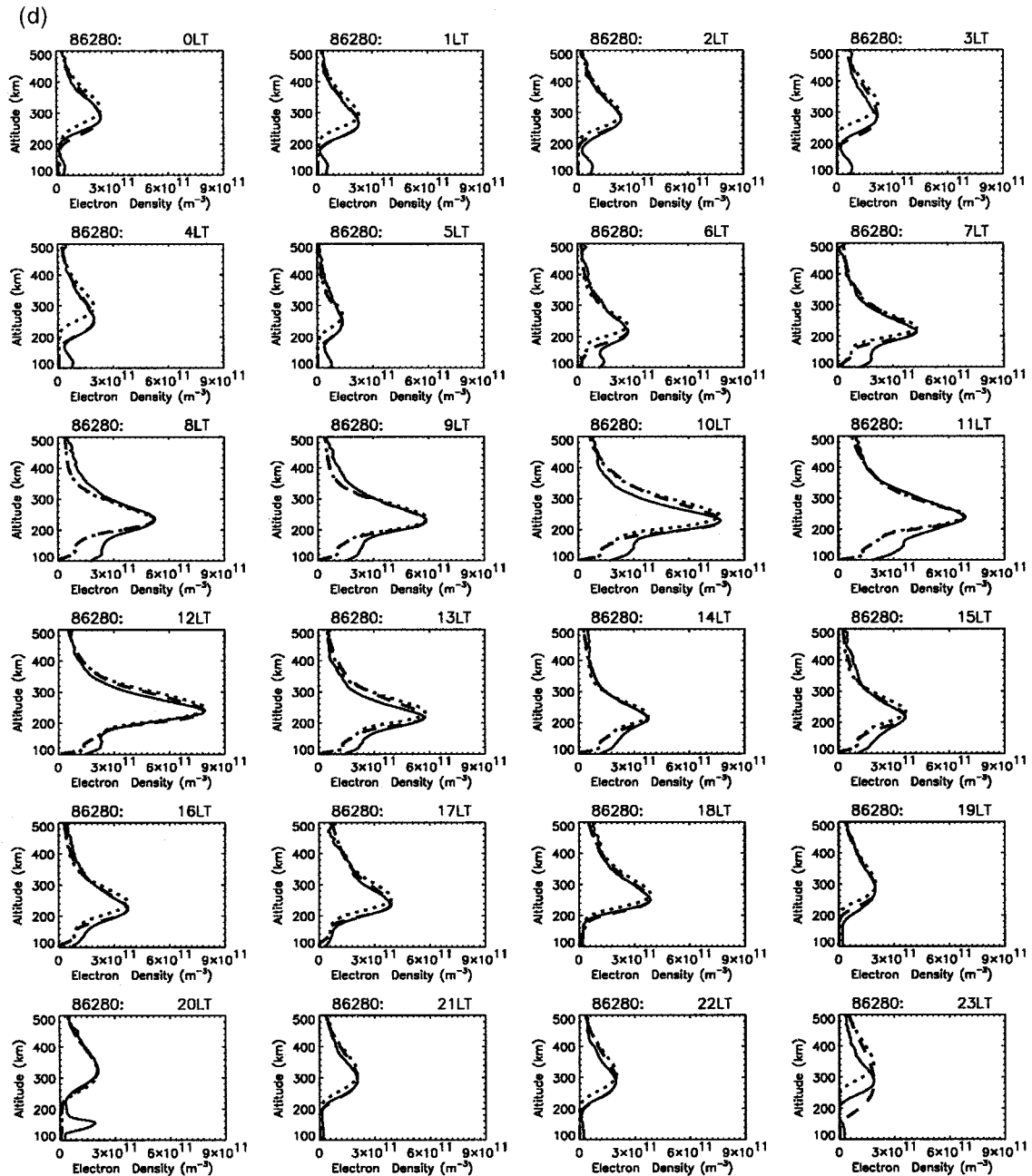


Fig. 2 (continued)

the AISOS term brings more reasonable agreement for  $h_m F2$ .

The  $N_m F2$  measurements reveal a rapid density increase around 08:00 LT, followed by a decrease at about 11:00 LT. This behavior is different from that predicted by IRI. Using either the  $v_z$ -based or  $h_m F2$ -based wind as input, the model cannot achieve the

lower electron density seen in the observations for 09:00–17:00 LT, if the neutral composition is specified by MSIS86 and the solar flux by EUV91. By night, the agreement in  $N_m F2$ , however, is improved when the  $h_m F2$ -based wind is applied. Obviously, to reproduce the observed  $N_m F2$  reasonably, model inputs of the background atmosphere or the EUV flux need to be

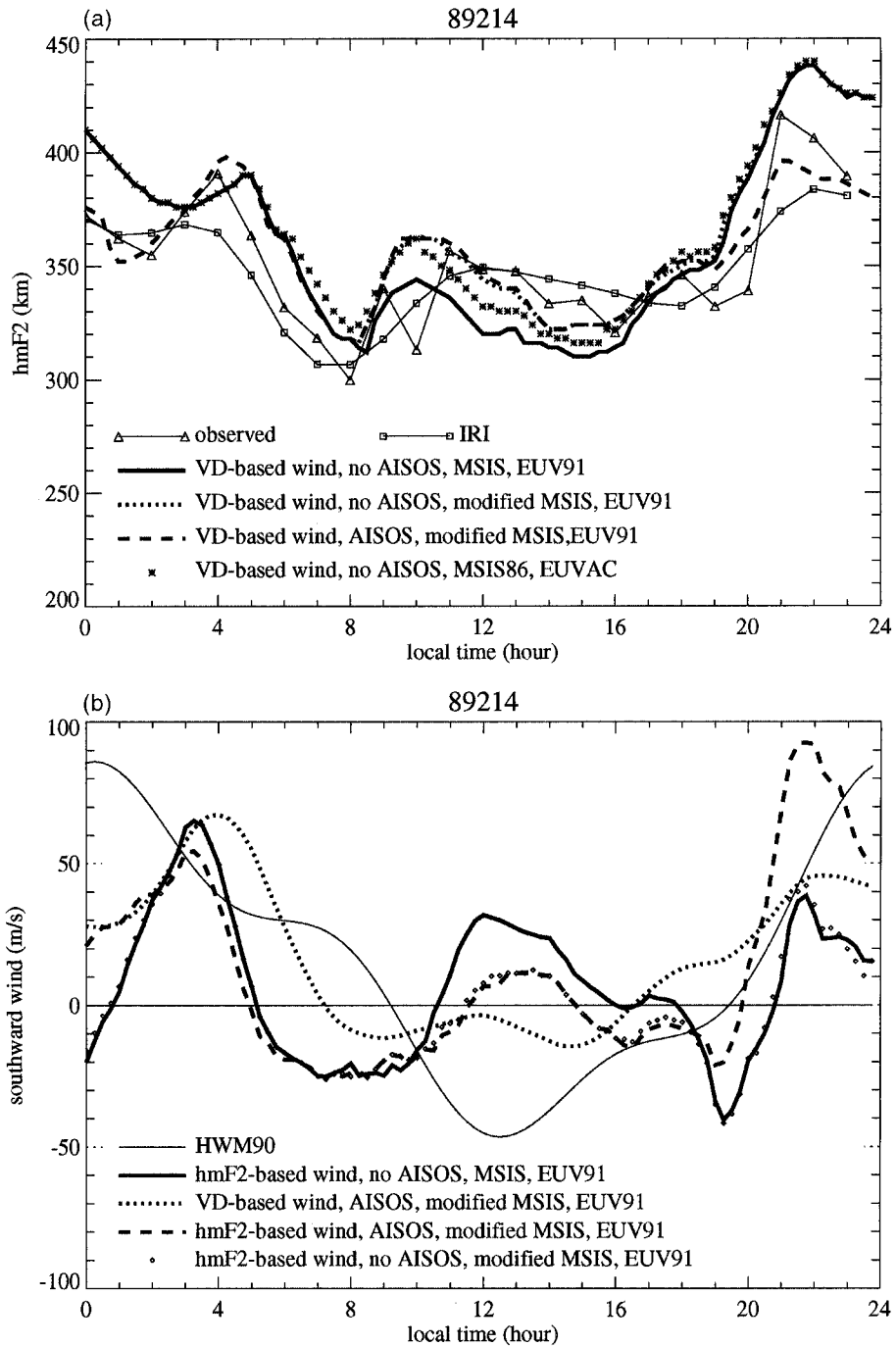


Fig. 3. Local time variations of (a)  $h_m F_2$ , (b) the equivalent southward wind and (c)  $N_m F_2$  for Case B (2 August 1989, day 89214). 'VD' stands for the measured vertical drift. 'AISOS' stands for additional ionization source or sink (see text).

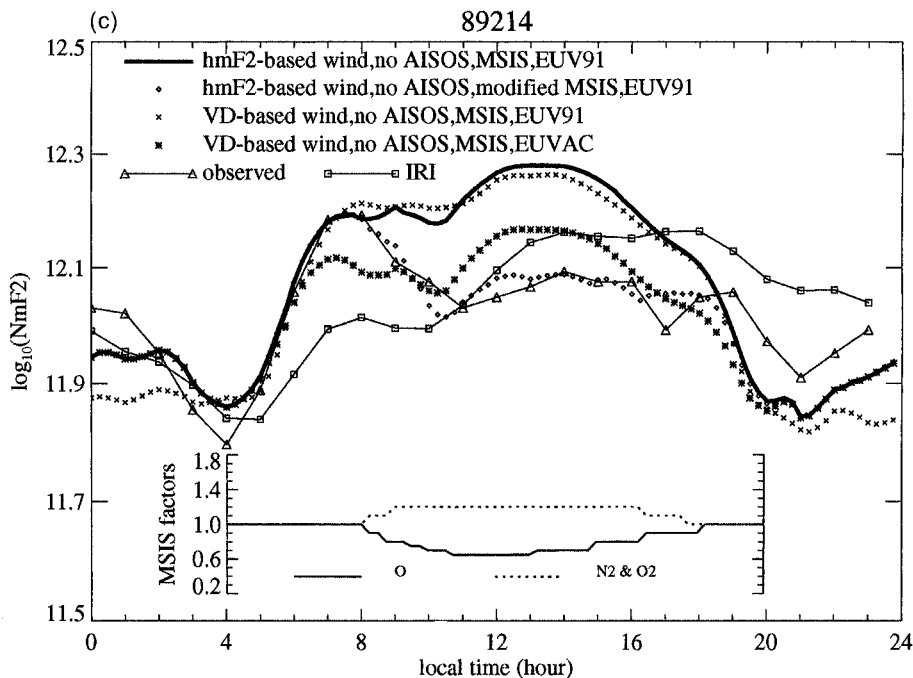


Fig. 3 (continued)

modified. By decreasing the MSIS O/N<sub>2</sub> ratio (Fig. 3(c)), i.e. decreasing O by up to 35% and increasing N<sub>2</sub> by up to 20%, the measured electron density can be well matched.

#### 4.3.2. Results for different EUV fluxes

EUV fluxes are poorly known. Tobiska (1993) found that measured E and F1 region electron densities are 30–50% above the values calculated using recent EUV models. This suggests a factor of ~2 error in the EUV model. For the F2 layer we find that EUV91 leads to higher densities than does EUVAC, but that the EUV91 densities match better with observations for low solar activity (Figs. 1(c) and 2(c)) while EUVAC densities match better for high solar activity (Figs. 3(c) and 4(c)). EUVAC also increases  $h_mF2$  by about 10 km at high solar activity.

#### 4.3.3. Wind

Fig. 3(b) shows the derived southward wind varies under different calculation conditions. The solid and dashed lines and diamonds are obtained using  $h_mF2$ -based winds. It can be seen that changes in the derived wind and in  $N_mF2$  are correlated, namely, (1) by day, the changes depend on whether MSIS is modified or not, contrary to our finding for Case B. A difference of about 30 m/s between the solid and dashed (or diamond) curves is seen; (2) by night, the changes depend

on whether an AISOS is introduced or not. A difference of about 30–50 m/s between the dashed and diamond curves is seen. The dotted line gives results obtained when  $v_z$ -based winds were used. The  $v_z$ -based and  $h_mF2$ -based winds show a similar trend of variation but with an offset of about 30–50 m/s in magnitude.

#### 4.4. Case D: 5 October 1989 (day 89278) equinox, high solar activity

##### 4.4.1. $h_mF2$

The observed  $h_mF2$  is generally 20–40 km higher than the IRI value, particularly before sunrise and around 10:00–17:00 LT, Fig. 4(a). The  $h_mF2$  modeling, with suitable modification to the MSIS O/N<sub>2</sub> ratio and AISOS, shows that the observed  $v_z$  seems able to account for the observed  $h_mF2$  variation (dashed line).

##### 4.4.2. Wind

The wind amplitude is found to be very small; especially during the day the  $v_z$ -based wind is only around 10 m/s, Fig. 4(b). As in Case C, if the MSIS composition is modified by day, the  $h_mF2$ -based wind weakens (diamonds and solid line), and if the AISOS is further included, the wind further weakens after 20:00 LT.

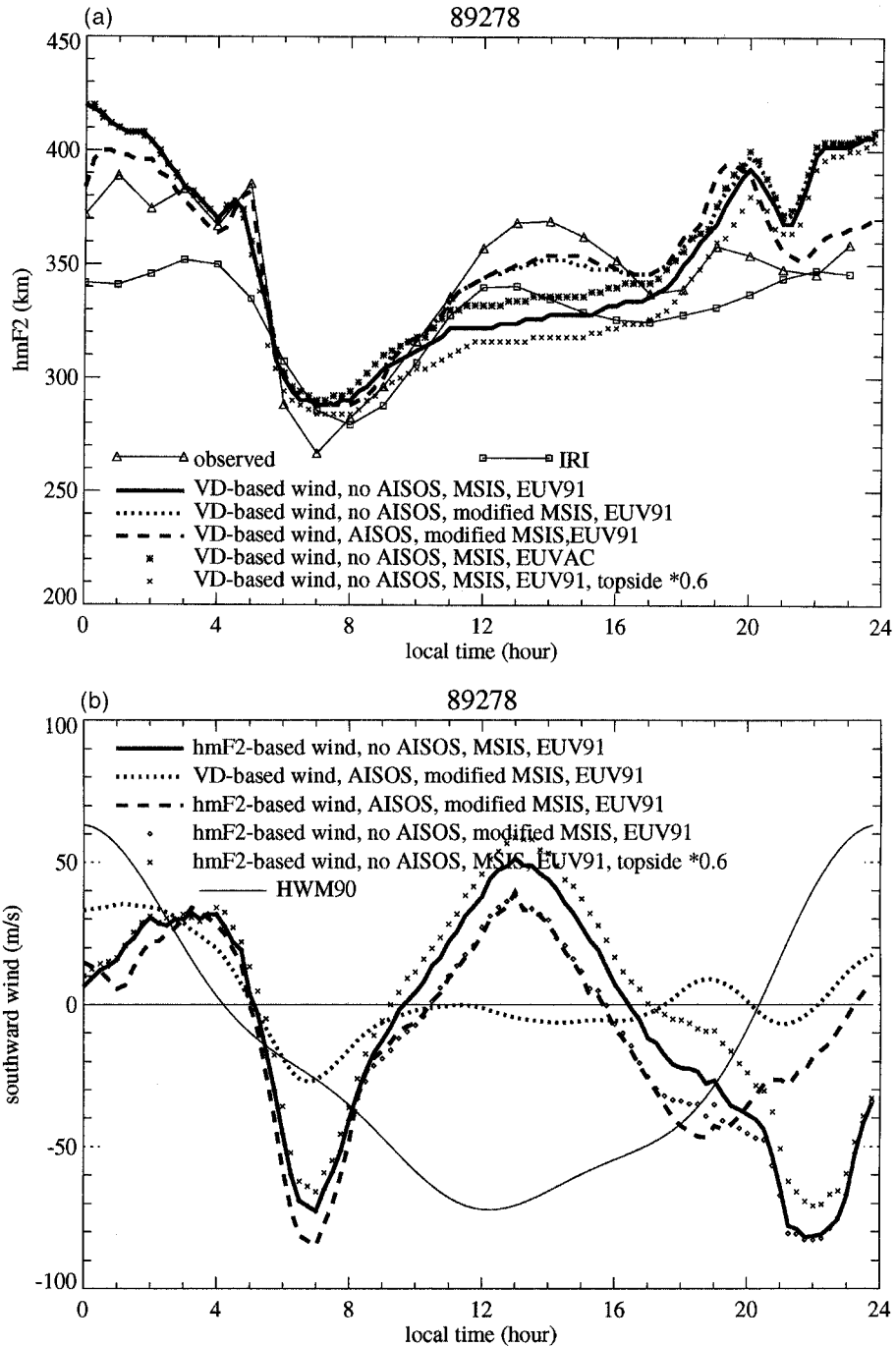


Fig. 4. Local time variations of (a)  $h_mF2$ , (b) the equivalent southward wind, (c)  $N_mF2$  and (d) the electron density profile for Case B (5 October 1989, day 89278). ‘VD’ stands for the measured vertical drift. AISOS stands for additional ionization source or sink (see text). The ‘topside \*0.6’ means that the  $O^+$  density at 500 km altitude is decreased by 40%. In (d), solid line: observation; dashed line: modeled with MSIS modification, ‘AISOS’,  $v_z$ -based wind; dotted line: the same as the dashed line except that the  $h_mF2$ -based wind is used.

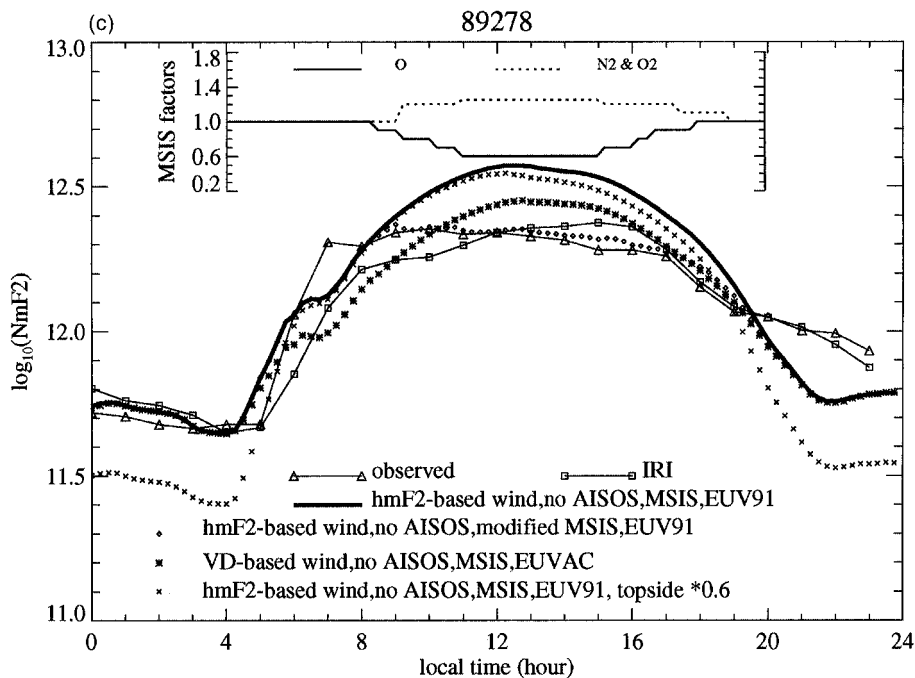


Fig. 4 (continued)

#### 4.4.3. $N_mF2$

The measured  $N_mF2$  is somewhat in accordance with the IRI value. If the model adopts EUVAC, no MSIS composition modification is required to match the measurements. If the model adopts EUV91, the MSIS O concentration needs to be decreased by up to 30% and  $N_2$  increased by 20% (see Fig. 4(c)).

#### 4.4.4. $N_e$ profile

It is interesting to note the comparisons of the measured electron density profile with the model ones (Fig. 4(d)). There is excellent agreement during the whole day; the bottom-side profiles are particularly well reproduced. The F1-layer density and the profile shape are very sensitive to the neutral concentration and EUV flux. Our inclusion of MSIS modifications and an AISOS (see further discussions later) seems successful in producing the whole profile from E to F2 region.

## 5. Further discussions and conclusions

The ionospheric modeling is highly dependent on various inputs which are not always readily available from observation. The critical inputs include the EUV flux (affecting the photoionization), the photoelectron impact (important for the bottom-side profile), atmospheric composition, temperature and winds, topside ionospheric exchange of ionization, and so on. We discuss these inputs later.

pheric composition, temperature and winds, topside ionospheric exchange of ionization, and so on. We discuss these inputs later.

### 5.1. Modeling $N_mF2$

We found in Case A that  $N_mF2$  variations can be reproduced by using the current MSIS composition model, the EUV91 model, and the radar drift measurements, particularly the  $v_z$  measurements. We state this as a general conclusion for low solar activity winter since data and model also agreed with the IRI (average) prediction for this case. For Cases B, C and D, we found discrepancies between the model and the data by day: at equinox for low solar activity the model value is smaller while for high solar activity it is greater. We were forced to invoke a MSIS modification or an AISOS or adopt a different EUV model to gain agreement for these cases.

#### 5.1.1. MSIS composition modification

It is generally believed that the standard MSIS model predicts thermospheric density to 15% accuracy (Hedin, 1987), but on any given day the prediction may be much worse. Although the four cases above are individual, we consider they are approximately representative as their maximum electron densities match IRI values well. Particularly for Case B, model-

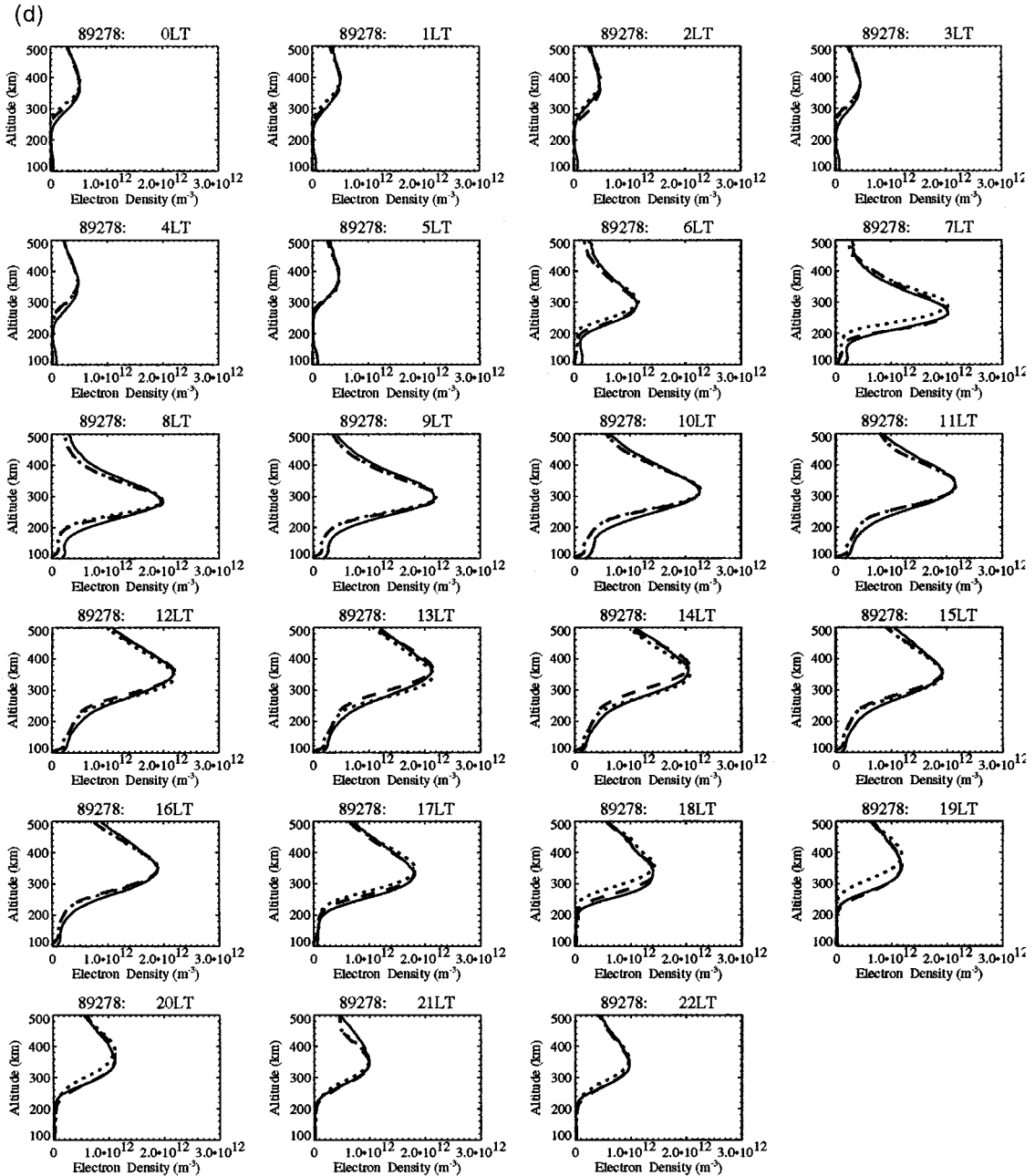


Fig. 4 (continued)

ing with either EUV91 or EUVAC suggests that the oxygen density was 40% higher than the MSIS prediction.

For high solar activity, Cases C and D, the  $O/N_2$  ratio was found to be smaller than that given by the MSIS model because modeling with either EUV model produced electron densities higher than those observed.

Actually, we cannot distinguish between electron density changes caused by composition changes and by EUV changes since decreasing the  $O/N_2$  ratio has the same effect as decreasing the EUV flux in reducing  $N_mF2$ . However, it can be said that for high solar activity, if EUV91 correctly specifies the EUV flux, then the true  $O/N_2$  ratio is substantially below the MSIS

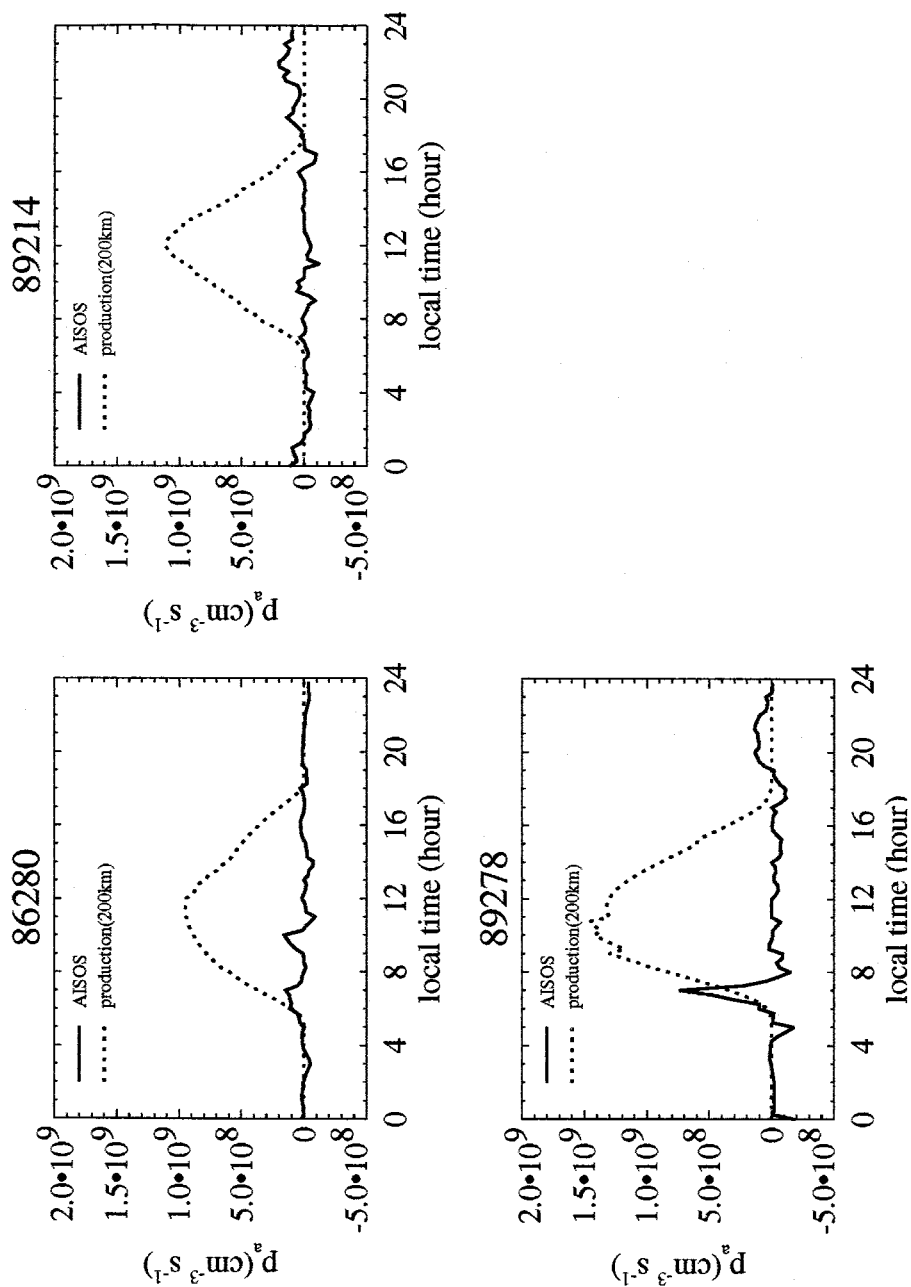


Fig. 5. Local time variations for the AISOS (additional ionization source or sink) (solid line) and  $\text{O}^+$  production rate at 200 km altitude (dotted line). They are obtained with the  $f_m F_2$ -based wind and MSIS modification as given in Figs. 2(c), 3(c) and 4(c). (a) Case B (15 December 1986, day 86349), (b) Case C (2 August 1989, day 89214), (c) Case D (5 October 1989, day 89278).

value while if EUVAC correctly specifies the EUV flux, then the true  $O/N_2$  ratio is much closer to the MSIS value.

We could further finely adjust the  $O/N_2$  ratio in time to minimize the model-data discrepancy, however, we would not expect the fast changes inevitably incurred to be realistic. During the night the effect of neutral-composition changes was not significant, and thus we opted to introduce the AISOS term.

### 5.1.2. Additional ionization source or sink: AISOS

When the model and measured  $N_mF2$  show small difference, we introduce the AISOS term. In Cases B, C and D this accompanies the primary modification of the MSIS concentrations. As shown for Case B in Fig. 5, the ratio of AISOS value  $p_a$  to the  $O^+$  production rate at 200 km  $p_0$  is usually less than 0.2 for the daytime; in Case C it is rather smaller; in Case D the AISOS is needed in the morning. In general, the additional ionization has to be provided during the night for high solar activity.

As stated before, we include the AISOS term just in order to make a fine adjustment of the model  $N_mF2$ . The AISOS is related to inadequate specifications in the modeling: (1) whether the MSIS, EUV91 and IRI models specify the neutral composition, the EUV flux, and the ionospheric temperatures adequately, whether the adopted reaction rate coefficients are correct, etc.; (2) whether a nighttime ionization source (usually ignored) needs to be added in some circumstances; (3) whether transient processes are important; (4) whether horizontal dynamics is important. In these regards, we can say that when we did use direct temperature measurements (Case D), model-data discrepancies remained, and also that temperature effects were found to be small compared with composition and EUV effects during the day but became important at night. Also, we have confirmed by comparing the four radar beams that horizontal gradients were small.

Actually, the AISOS is introduced not to sort out the physical reasons for the model-data difference but to examine how the wind deductions from  $h_mF2$  and from drift data are affected when the measured  $N_mF2$  and  $N_e$  profile are or are not well reproduced. The improved accuracy of the model electron density produced with the AISOS allows for more accurate ionosphere/thermosphere studies. Such close agreement is also an important requirement for the wind deduction from the measured drift data, since it may provide an accurate estimation of the ion diffusion drift. The diffusion drift depends on the height gradient of the ion density, which is not always available simultaneously with the drift measurements in MU radar experiments.  $N_mF2$  is always obtained from the ionosonde. The AISOS term is included to adjust the calculated  $N_mF2$ , and, as shown in Figs 2(d) and 4(d), our model can

bring excellent agreement between data and model over the whole electron density profile. The AISOS method, therefore, provides a useful approach convenient to derive the meridional wind when only  $N_mF2$ , instead of the  $N_e$  profile, is available.

### 5.1.3. EUV flux

It was found that the EUVAC model results in lower  $N_mF2$  than does the EUV91 model, slightly worsening the model and measurement agreement for low solar activity but improving the agreement for high solar activity.

## 5.2. Modeling $h_mF2$ and deriving winds

Our modeling of the MU radar measurements indicates that the vertical drift can be used to explain the general behavior of  $h_mF2$ . The wind derived from  $h_mF2$  with the help of those theoretical model resembles approximately in trend the wind obtained from the vertical drift data. However, for a few conditions, e.g. during sunrise and sunset, the ionospheric temperatures and the ionization production experience rapid changes with time and latitude, and the  $h_mF2$ -based wind may not be determined solely by the thermospheric wind and/or electric field.

For the low solar activity case, especially for Case A, fluctuations in the  $h_mF2$ -based wind are larger than those in the original  $h_mF2$  data.  $h_mF2$  is lower for low solar activity, usually below 230 km by day, where the  $O^+$  lifetime  $1/\beta$  is much shorter than it is at higher altitudes. Transport is important if it moves the ionization through one scale height within its lifetime (Rishbeth and Garriott, 1969); therefore, at lower altitudes, the wind effect is less important. The ionospheric peak height is not so sensitive to wind changes for low solar activity.

The model calculation is sometimes unable to reproduce  $N_mF2$  and the  $h_mF2$ -based wind. Like  $N_mF2$ ,  $h_mF2$  variations are affected by a variety of causes. It is interesting to understand how the derived wind is affected when electron density is not reliably modeled. We discuss this in terms of the neutral composition, AISOS term, EUV flux and top boundary  $N_e$ , all important model factors.

### 5.2.1. Atmospheric concentration

We have found it necessary to make modifications to the MSIS  $O/N_2$  ratio for both low and high solar activity in order to achieve agreement in  $N_mF2$ . The calculated  $h_mF2$  is found to increase significantly as the ratio decreases for high solar activity but to vary little for low solar activity. These composition modifications change both the chemical and diffusion lifetimes of the ionization and consequently establish a new balance height ( $h_mF2$ ) at which these lifetimes are

comparable. The corresponding changes in the  $h_mF2$ -based wind are around 20 m/s for high solar activity but much smaller for low solar activity (see the solid lines and diamonds in Figs. 2(b), 3(b) and (4)). The exact consequence, of course, depends on the amount of the modifications as well as solar activity.

### 5.2.2. Additional ionization source or sink: AISOS

By comparing the diamond curves and dashed lines in Figs. 2(b), 3(b) and 4(b), we find that after adjusting the AISOS to yield close agreement between model and data  $N_mF2$ , the derived wind experiences changes being larger (by more than 50 m/s) by night and smaller by day, depending also on the magnitude of the AISOS term.

### 5.2.3. EUV flux

If we adopt the MSIS model composition, the EUVAC model gives a lower F2-layer density but a higher  $h_mF2$  (by several km for low solar activity but more than 10 km for high solar activity) than does the EUV91 model. This is caused by a faster decrease in  $O^+$  production toward lower altitudes (so that the height of maximum  $O^+$  production forms at a higher altitude) for the EUVAC model.

### 5.2.4. Topside $N_e$ concentration

It is well understood that the upper  $O^+$  concentration controls  $N_mF2$  strongly in a model simulation, but it is not clear if the wind deduction from  $h_mF2$  is influenced also. All of the above case studies have used the electron density observed at 500 km altitude as the model upper boundary condition. To understand the effect of the value adopted for the upper boundary condition, we imposed a 40% decrease in the measured electron density at 500 km throughout the 24 h for Case D. No MSIS or AISOS adjustment was used. We found that  $N_mF2$  decreased by about 11% during the day, when photoionization strongly governs ionospheric structure, and by about 40% by night, when there is no photoionization (see the crosses in Fig. 4(c)). This day–night difference confirms the importance of an upper-boundary ionization flux in maintaining the nighttime ionosphere, as found previously (e.g. Park and Banks, 1975).

It is also found that the  $h_mF2$ -based wind increases by less than 20 m/s by day as a result of the  $N_e$  decrease at the top boundary, and by a much smaller amount by night although  $N_mF2$  decreases a lot. The model  $h_mF2$  is lowered by less than 15 km by day and virtually not influenced by night (see the solid line and crosses in Fig. 4(a) when the  $v_z$ -based wind is used to calculate  $h_mF2$ ). Therefore, knowledge of  $N_mF2$  alone is not sufficient to infer the meridional wind; the upper-boundary condition must be known as well, as was concluded by Sica et al. (1990). Inferring winds

from  $h_mF2$ , however, suffers little from the uncertainty in the upper fluxes at midlatitudes during the nighttime, but during the day the inference suffers by an amount comparable with that due to the uncertainty in neutral composition.

The preceding discussions indicates that when the modeled  $N_mF2$  does not match observations, the uncertainty of the  $h_mF2$ -based winds derived with the help of a theoretical model can be around 20–30 m/s by day, and this uncertainty is due mainly to the uncertainties in the neutral composition and top boundary concentrations. The wind uncertainty ranges up to 50 m/s by night, and this is due mainly to the uncertainty in the nighttime ionization source.

As for the disagreement between the  $h_mF2$ -based and the  $v_z$ -based winds, there are two possible reasons. (1) We have used drift measurements averaged over 220–350 km or 200–450 km altitude, where the diffusion velocity varies fast with altitude, thus the ionization at different altitudes may not respond to wind changes at the same rate. In fact, the  $h_mF2$ -based wind is applicable mainly around the F2 peak. (2) In Cases A and D,  $h_mF2$  and the drift data were not collected on the same days.

## 6. Summary

We have reported initial results of data modeling and assimilation studies for several MU radar experiments of the power, ion-drift and temperature profiles. We have investigated quantitatively the effects of different drift components, of changes in atmospheric composition, of changes in solar EUV flux and of changes in the upper  $O^+$  density boundary condition on the model electron density ( $N_mF2$ ,  $h_mF2$  and the  $N_e$  profile). We have also discussed neutral wind calculations and the uncertainty of the empirical MSIS86 and EUV flux model predictions. As an initial step in the study of data assimilation into our model, this investigation addressed model sensitivity to various inputs; it does not yet address the uniqueness with which the contributions may be determined. It explores the extraction of the physics from the data but does not yet attempt forecasting from these deductions.

The midlatitude ionospheric model used in this study takes account of the main dynamic and photochemical processes controlling the behavior of  $O^+$ ,  $NO^+$ ,  $O_2^+$  and  $N_2^+$  in the ionospheric E- and F-regions. The upper boundary condition is  $O^+$  density, which is available from the IRI model or radar observations or obtained by matching the observed maximum electron density  $N_mF2$ . The experimental vertical plasma drift may be applied directly to simulate the vertical motion of  $O^+$ ; the model can also calculate and use an equivalent neutral wind based by reprodu-

cing the observed height of the F2 peak  $h_mF2$ . The model maximum electron density  $N_mF2$  can be forced to match the observed value by introducing an additional ionization source or sink (AISOS).

Four cases have been analyzed: 15 December 1986 (Case A), 7 October 1986 (Case B), 2 August 1989 (Case C) and 5 October 1989 (Case D). These individual cases can be considered approximately representative for their respective solar activity and season in the sense that their  $h_mF2$  and  $N_mF2$  values approximate those of the IRI.  $h_mF2$  modeling is carried out with drift measurements as input;  $N_mF2$  modeling is carried out with the model  $h_mF2$  constrained to the observed values by using an equivalent wind. Two types of meridional wind have been obtained from the MU radar data, that deduced directly from the line-of-sight velocity measurements and that deduced from the altitude of peak electron density  $h_mF2$ . Different aspects of the modeling have been discussed for the four cases. In Case A the consequences of using the full vertical drift as opposed to only the vertical component of the parallel drift are assessed; in Case B the consequences of modifying the MSIS model neutral concentration are assessed; in Case C the consequences of different EUV flux models are assessed; in Case D, the consequences of adjusting the top-boundary  $O^+$  density boundary condition are assessed.

It was found that (1) the measured ion drift (particularly the vertical drift) can explain quantitatively well the measured  $h_mF2$  (particularly at low solar activity), while the  $h_mF2$ -based wind gave more reasonable  $N_e$  model results than did direct application of the measured drifts; (2) atmospheric  $O/N_2$  changes result in not only changes in  $N_mF2$  but also in  $h_mF2$ : for high solar activity,  $h_mF2$  increases as  $O/N_2$  decreases; (3) the difference in the EUV91 and the EU-VAC models at high solar activity causes significant differences in model  $N_mF2$  and  $h_mF2$  (by about 10 km); (4) while the upper-boundary  $O^+$  density affects  $N_mF2$  more by night than by day, it affects  $h_mF2$  little by night and by about 10 km by day; (5) related to the conclusions (2)–(4), we note that the meridional wind needed by the model to reproduce the observed  $h_mF2$  differed according to how well the model reproduced the observed  $N_mF2$ .

An additional ionization source or sink (AISOS) term is applied in the model to bring the model  $N_mF2$  into exact agreement with the measurements, so as to examine whether the  $h_mF2$ -based and  $v_z$ -based winds are affected when the measured  $N_mF2$  is or is not reproduced well. We found that the winds do differ, though we cannot sort out the physical reasons for the model-data difference.

The uncertainty in the MSIS86 and EUV model predictions have also been discussed. We found that, if the MSIS and EUV91 models are applied, the model

gives an  $N_mF2$  for high solar activity higher than the measured one. Thus the MSIS  $O/N_2$  ratio needs to be reduced if EUV91 is applied for modeling, while, if EUVAC is applied, there is little need for such modification. For equinox at low solar activity, modeling with either EUV model produces lower  $N_mF2$ , and the  $O/N_2$  ratio may likely be higher than given by the MSIS model.

## Acknowledgements

The MU radar belongs to and is operated by the Radio Atmospheric Science Center (RACS) of Kyoto University. One of the authors (S.R.Z) was supported by the COE program of the Ministry of Education, Science, Sports and Culture of Japan. During the model construction, S.R.Z obtained support from the National Natural Science Foundations of China. The IRI90 model was kindly provided by Dr D. Bilitza, and the EUV91, EUVAC, MSIS86 and HWM90 models were obtained from NSSDC, GSFC. The drift/temperature and the electron density data are from databases created by Drs Y. Otsuka and T. Takami.

## References

- Balan, N., Otsuka, Y., Fukao, S., 1997. New aspects in the annual variation of the ionosphere observed by the MU radar. *Geophysical Research Letters* 24, 2,287–2,290.
- Banks, P., 1966. Collision frequencies and energy transfer: ions. *Planetary and Space Sciences* 14, 1105–1122.
- Bilitza, D. 1990. International reference ionosphere 1990, National Space Science Data Center/World Data Center A for Rockets and Satellites, 90–22.
- Buonsanto, M.J., 1995. Millstone Hill incoherent scatter F region observations during the disturbance of June 1991. *Journal of Geophysical Research* 100, 5,743–5,755.
- Buonsanto, M.J., Solomon, S.C., Tobiska, W.K., 1992. Comparison of measured and modeled solar EUV flux and its effect on the E–F1 region atmosphere. *Journal of Geophysical Research* 97, 10,513–10,524.
- Buonsanto, M.J., Starks, M.J., Titheridge, J.E., Richards, P.G., Miller, K.L., 1997. Comparison of techniques for derivation of neutral meridional winds from ionospheric data. *Journal of Geophysical Research* 102, 14,477–14,484.
- Buonsanto, M.J., Salah, J.E., Miller, K.L., Oliver, W.L., Burnside, R.G., Richards, P.G., 1989. Observations of neutral circulation at mid-latitude during the equinox transition study. *Journal of Geophysical Research* 94, 987–997.
- Fukao, S., Takami, T., Oliver, W.L., 1996. The coupled ionosphere and thermosphere at mid-latitudes in the Asian Sector and its comparison with other locations. *Journal of Geomagnetism and Geoelectricity* 48, 113–124.
- Fukao, S., Sato, T., Tsuda, T., Yamamoto, M., Kato, S., 1990. The MU radar: new capabilities and system calibrations. *Radio Science* 25, 477–485.

- Hedin, A.E., 1987. MSIS-86 thermospheric model. *Journal of Geophysical Research* 92, 4649–4662.
- Hedin, A.E., 1988. Atomic oxygen modeling in the upper thermosphere. *Planetary Space Sciences* 36, 907.
- Hedin, A.E., Biondi, M.A., Burnside, R.G., Hernandez, G., Johnson, R.M., Kileen, T.L., Mazaudier, C., Meriwether, J.W., Salah, J.E., Sica, R.J., Smith, R.W., Spencer, N.W., Wickwar, V.B., Virdi, T.S., 1991. Revised globe model of thermospheric winds using satellite and ground-based observations. *Journal of Geophysical Research* 96, 7657–7688.
- Igi, S., Ogawa, T., Oliver, W.L., Fukao, S., 1996. Thermospheric wind over Japan: comparison of ionosonde and radar measurements. *Journal of Geophysical Research* 100, 21,323–21,326.
- Lilosten, J., Kofman, W., Wisenberg, J., Oran, E.S., Devore, C.R., 1989. Ionization efficiency due to primary and secondary photoelectrons: a numerical model. *Annales Geophysicae* 7 (1), 83–90.
- Mikhailov, A.V., Foster, J.C., 1997. Daytime thermosphere above Millstone Hill during severe geomagnetic storms. *Journal of Geophysical Research* 102, 17,275–17,282.
- Miller, K.L., Lemon, M., Richards, P.G., 1997. A meridional wind climatology from a fast model for the derivation of meridional winds from the height of the ionospheric F2 region. *Journal of Atmospheric and Solar-Terrestrial Physics* 59, 1,805–1,822.
- Miller, K.L., Torr, D.T., Richards, P.G., 1986. Meridional winds in the thermosphere derived from measurements of layer height. *Journal of Geophysical Research* 91, 4531–4535.
- Mitra, A.P., 1968. A review of D-region processes in non-polar latitudes. *Journal of Atmospheric and Terrestrial Physics* 30, 1,065–1,114.
- Oliver, W.L., Grotfelty, K., 1996. O<sup>+</sup>-O collision cross section and long-term F region O density variations deduced from the ionospheric energy budget. *Journal of Geophysical Research* 101, 21,769–21,784.
- Oliver, W.L., Yamamoto, Y., Takami, T., Fukao, S., Yamamoto, M., Tsuda, T., 1993. Middle and upper atmosphere radar observations of ionospheric electric fields. *Journal of Geophysical Research* 98, 11,615–11,627.
- Park, C.G., Banks, P.M., 1975. Influence of thermal plasma flow on the daytime F2-layer. *Journal of Geophysical Research* 80, 2819–2823.
- Pavlov, A.V., Buonsanto, M.J., 1997. Comparison of model electron densities and temperatures with Millstone Hill observations during undisturbed periods and the geomagnetic storms of 16–23 March and 6–12 April 1990. *Annales Geophysicae* 15, 327–344.
- Richards, P.G., 1991. An improved algorithm for determining neutral winds from the height of the F2 peak electron density. *Journal of Geophysical Research* 96, 17,839–17,846.
- Richards, P.G., Torr, D.G., 1988. Ratios of photoelectron to EUV ionization rates for aeronomic studies. *Journal of Geophysical Research* 93, 4060–4066.
- Richards, P.G., Wilkinson, P.J., 1998. The ionosphere and thermosphere at southern midlatitudes during the November 1993 ionospheric storm: a comparison of measurement and modeling. *Journal of Geophysical Research* 103, 9,373–9,389.
- Richards, P.G., Fennelly, J.A., Torr, D.G., 1994a. EUVAC: A solar EUV flux model for aeronomic calculations. *Journal of Geophysical Research* 99, 8981–8992.
- Richards, P.G., Torr, D.G., Hagan, M.E., Buonsanto, M.J., 1995. A new algorithm for improved ionospheric electron density modeling. *Geophysical Research Letters* 22, 1,385–1,388.
- Richards, P.G., Torr, D.G., Reinisch, B.W., Gamache, R.P., Wilkinson, P.J., 1994b. F2 peak electron density at Millstone Hill and Hobart: comparison of theory and measurement at solar maximum. *Journal of Geophysical Research* 99, 15,005–15,016.
- Rishbeth, H., Fukao, S., 1995. A review of MU radar observations of the thermosphere and ionosphere. *Journal of Geomagnetism and Geoelectricity* 47, 621–637.
- Rishbeth, H., Garriott, O.K., 1969. *Introduction to Ionospheric Physics*. Academic Press, New York and London.
- Rishbeth, H., Ganguly, S., Walker, J.C.G., 1978. Field-aligned and field-perpendicular velocities in the ionospheric F2-layer. *Journal of Atmospheric and Terrestrial Physics* 40, 767–784.
- Rishbeth, H., Jenkins, B., Moffett, R.J., 1995. The F-layer at sunrise. *Annales Geophysicae* 13, 367–374.
- Sato, T., Ito, A., Oliver, W.L., Fukao, S., Tsuda, T., Kato, S., Kimura, I., 1989. Ionospheric incoherent scatter measurements with the middle and upper atmospheric radar: techniques and capability. *Radio Science* 24, 85–98.
- Sica, R.J., Schunk, R.W., Wilkinson, P.J., 1990. A study of the undisturbed mid-latitude ionosphere using simultaneous multiple site ionosonde measurements during the Sundial-86 campaign. *Journal of Geophysical Research* 95, 8,271–8,279.
- Su, Y.Z., Fukao, S., Bailey, G.J., 1997. Modeling studies of the middle and upper atmosphere radar observations of the ionospheric F layer. *Journal of Geophysical Research* 102, 319–327.
- Titheridge, J.E., 1993. Atmospheric winds calculated from diurnal changes in the mid-latitude ionosphere. *Journal of Atmospheric and Terrestrial Physics* 55, 1637–1659.
- Titheridge, J.E., 1996. Direct allowance for the effect of photoelectrons in ionospheric modeling. *Journal of Geophysical Research* 101, 357–369.
- Tobiska, W.K., 1991. Revised solar extreme ultraviolet flux model. *Journal of Atmospheric and Terrestrial Physics* 53, 1005–1018.
- Tobiska, W.K., 1993. Recent solar extreme ultraviolet irradiance observations and modelling: a review. *Journal of Geophysical Research* 98, 18879–18990.
- Torr, D.G., Torr, M.R., 1979. Chemistry of the thermosphere and ionosphere. *Journal of Atmospheric and Terrestrial Physics* 41, 797–839.
- Torr, M.R., Torr, D.G., 1982. The role of metastable species in the thermosphere. *Reviews of Geophysics and Space Physics* 20, 91–144.
- Zhang, S.-R., Huang, X.-Y., 1995. A numerical study of ionospheric profiles for mid-latitudes. *Annales Geophysicae* 13, 551–557.
- Zhang, S.-R., Huang, X.-Y., Su, Y.-Z., Radicella, S.M., 1993. A physical model for one-dimensional and time-dependent

ionosphere—part I: description of the model. *Annali di Geofisica* 36, 105–110.  
Zhang, S.-R., Zhang, M.-L., Radicella, S.M., Huang, X.-Y.,

Bilitza, D., 1996. A comparison of the lower transitions height obtained with a theoretical model and with IRI. *Advances in Space Research* 18, (6)165–(6)173.